npj | 2D Materials and Applications

ARTICLE OPEN

Bottom-up water-based solution synthesis for a large MoS_2 atomic layer for thin-film transistor applications

Young-Jin Kwack[1,2], Thi Thu Thuy Can[1,2] and Woon-Seop Choi[1]✉

A bottom-up water-based solution-process method was developed for atomic layered MoS_2 with a one-step annealing process and no sulfurization. The chosen MoS_2 precursor is water soluble and was carefully formulated to obtain good coating properties on a silicon substrate. The coated precursor was annealed in a furnace one time to crystallize it. This method can obtain a large and uniform atomic layer of 2D MoS_2 with 2H lattice structure. The number of atomic layers (4–7) was controlled through the precursor concentrations and showed good uniformity, which was confirmed by STEM and AFM. Four types of thin-film transistors (TFTs) were prepared from the solution-processed MoS_2 on Al_2O_3 and SiO_2 dielectric with either thermal evaporated Al or printed Ag source and drain electrodes. The best result shows an improved mobility of 8.5 $cm^2 V^{-1} s^{-1}$ and a reasonable on–off ratio of about 1.0×10^5 with solid output saturation.

npj 2D Materials and Applications (2021)5:84 ; https://doi.org/10.1038/s41699-021-00264-7

INTRODUCTION

Transitional metal dichalcogenide (TMDC) has a hexagonal structure with one layer of IV, V, and VI transitional atom (M) between two layers of chalcogen atoms (X). M–X combinations result in strong covalent bonds, while the adjacent layers have Van der Waals bonds, allowing for separation between layers[1]. TMDCs have a band gap that is tunable from 1 eV (bulk) to 2 eV (monolayer) and are promising for transistors, optoelectronic devices, and future electronic devices[2]. The most actively studied TMDC substance is molybdenum disulfide (MoS_2).

There have been many methods to make two-dimensional (2D) TMDC materials that can be categorized into top–down and bottom–up. The top–down methods start from bulk MoS_2 crystal form as the raw material such as mechanical exfoliation, chemical exfoliation, and ultra-sonication based on the weak interlayer Van der Waals force. Though simple, these methods have such drawbacks like small scale, random shape, and hard-controlled thickness, thus limiting their practical applications. Comparably, bottom–up methods that have high quality, controllable layer number and scale can be classified into chemical vapor deposition (CVD) or metal oxide (MO) CVD[3–5] and solution-processed routes.

CVD is the most commonly studied way to synthesize MoS_2 on a large scale. However, this method requires a sulfurization process where sulfur powder is placed in a furnace to facilitate the embedding of sulfur atoms in the 2D lattice structures. The toxic materials used in this method are a weakness when manufacturing.

Solution processes for 2D materials are developed due to the advantages of a simpler method, high throughput, large size, and low cost with an environmentally friendly process. Among those processes, ammonium tetrathiomolybdate ($(NH_4)_2MoS_4$) precursor was used to make a MoS_2 thin film by dip coating[6]. However, this method needed a two-step thermolysis with an expensive sapphire substrate and was not totally applicable to large-area preparation. Another approach was to use a mixed solvent system to obtain MoS_2 layers by a solution process[7–9], where a two-step annealing process and sulfurization or pulsed laser annealing were also required.

Our group has focused on solution processes that do not require sulfurization. A unique solution process was reported using $(NH_4)_2MoS_4$ precursor without CVD[10]. The first key point was making the 2D MoS_2 precursor solution by developing a new sulfur-rich solution and making thin film coatings with good wetting properties. The second point was growing MoS_2 atomic layers without sulfurization in a one-step annealing process to obtain a 2H MoS_2 structure[10]. Most recently, direct patterning of MoS_2 layer was also developed without sulfurization[11].

In this study, a deionized (DI) water-based solution process was developed for MoS_2 thin film by bottom–up thermolysis method for the first time. This method was relatively easy to handle, safe, and environmentally friendly because water was used as one of the main solvents. A new MoS_2 formulation was prepared with the addition of sulfur to the ammonium molybdate tetrahydrate ($(NH_4)_6Mo_7O_{24}{\cdot}4H_2O$) precursor. The MoS_2 film was also completed without sulfurization and with a single step of annealing, as additional sulfur vapor did not need to be delivered for the sulfurization process because of its sulfur-rich solution. This method for synthesizing MoS_2 distinguished our work from others[6–9].

This synthesized MoS_2 layer was used as a semiconductor in thin-film transistors (TFTs) with Al or Ag source and drain (S/D) electrodes instead of Au/Ti system[10,12]. Applying printed electrodes for the contacts on solution-processed MoS_2 is interesting because of the possibility of large-area electronics with low costs and an environmentally friendly printing process. Electrohydrodynamic (EHD) jet printing is a good candidate for printing Ag paste regardless of the materials' viscosity[13]. We fabricated spin-coated MoS_2 TFTs with a high yield, with either thermally evaporated Al or EHD jet-printed Ag S/D electrodes, along with SiO_2 or Al_2O_3 gate dielectrics to provide four types of TFTs, as shown in Fig. 1. Eventually, the TFT group with the combination of high-*k* Al_2O_3 and Al shows improved performance in electron mobility and in on-to-off current ratio. Our work suggests that this methodology

[1]School of Electronics and Display Engineering, Hoseo University, Asan 31499, Korea. [2]These authors contributed equally: Young-Jin Kwack, Thi Thu Thuy Can. ✉email: wschoi@hoseo.edu

npj nature partner journals

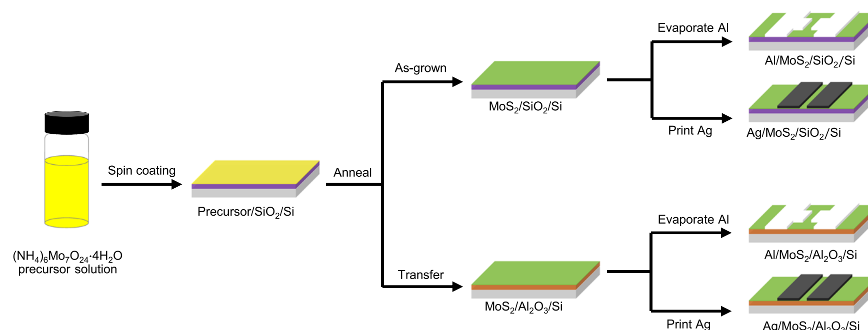

Fig. 1 Fabrication process of MoS_2 TFTs. Fabrication process of MoS_2 TFTs with thermal evaporated Al (top) and EHD jet printing technique (bottom) with SiO_2 and Al_2O_3.

can be applied to multifarious devices and has the potential for scalability in 2D materials.

RESULTS

Development of a new precursor solution

To prepare solution-processed MoS_2, previous studies used $(NH_4)_2MoS_4$ as a precursor and faced difficulties in coating uniformity due to the surface tension of ionic thiomolybdate (MoS_4^{2-}) clusters[7]. In general, sulfur-flux (sulfurization) processes are necessary because sulfur is lost during annealing, even though the sulfur is dissolved in the precursor formulation. In this work, $(NH_4)_6Mo_7O_{24}{\cdot}4H_2O$ as Mo source was employed. DI water was chosen as a solvent for preparing the Mo precursor solution due to it being easily found, inexpensive, non-toxic, and environmentally friendly. The S source was important in making our work dissimilar from CVD methods as we combined the S source solution with the Mo solution. CVD methods instead places the S powder inside the furnace during high-temperature annealing. The advantage of using all precursors in the liquid phase is to prevent the uncontrollable flow of powder in the furnace.

While $(NH_4)_6Mo_7O_{24}{\cdot}4H_2O$ is dissolved well in water, sulfur could not be dissolved in numerous solvents such as water or alcohol and only dissolves in small amounts in amine derivatives. Even though CS_2 is a good solvent for sulfur, CS_2 solution does not show good wetting on a SiO_2 substrate. As CS_2 has a low boiling point of 46.3 °C, it constantly evaporates at room temperature, and it is not possible to use the solvent alone. CS_2 can be mixed well with ethanolamine to dissolve sulfur to prepare S source. Therefore, a sulfur-containing MoS_2 precursor solution was formulated with CS_2, ethanolamine, and DI water. The solvents used in the solution are some of the major factors in the coating condition. Therefore, the ratio of DI water as a solvent in the Mo's precursor and ethanolamine as a solvent of sulfur greatly affects the coating state on the wafer substrate.

After several formulation studies, Mo precursor and sulfur solutions were prepared at ratios of 3:1–1:3 to check the wetting and coating conditions. All solutions were mixed well and showed good stability. However, the coating states of the different solution mixtures on the silicon wafer were different (Supplementary Fig. 1a). If the ratio of DI water-based solution is high, pin holes and wrinkling occur, resulting in an uneven coating layer. This is unfit for spin-coating since the sulfur and CS_2 do not dissolve in DI water at all.

The most uniform thin film occurred at a ratio of 1:2. We measured the contact angle on the SiO_2 substrate after ultraviolet (UV)/O_3 treatment for 30 min, and it seemed that stable coating was possible due to the good wetting characteristics at a contact angle of 4.0° (Supplementary Fig. 1b). Based on this, the final solution was prepared with a Mo:S atomic ratio of 1:2.

Two precursor solutions were prepared with and without CS_2 to find out how the CS_2 affects the coating conditions of the sulfur solution. Supplementary Fig. 1c shows the state of the solution before and after adding CS_2 to the mixture of sulfur and ethanolamine. If the ethanolamine is added with sulfur, it starts to melt very slowly and gradually turns green, and there is no visible sediment, but the solution turns deep green. When adding CS_2 in the mixture, it turns transparent yellow within seconds.

These two solutions were mixed with a DI water-based $(NH_4)_6Mo_7O_{24}{\cdot}4H_2O$ solution and spin-coated on SiO_2. The layer without CS_2 was highly patterned due to uncovered part of the surface (Supplementary Fig. 1d). With the addition of CS_2, a clear coating of $(NH_4)_6Mo_7O_{24}{\cdot}4H_2O$ precursor solution could be obtained (Supplementary Fig. 1e). After the precursor solution was spin-coated on a silicon wafer, the films were soft baked at 150 °C for 30 min and thermally annealed at 500–1000 °C in a furnace for 1 h. Sulfurization in CVD was not necessary in this method.

Characterization of MoS_2 thin films

Figure 2a shows the Raman spectra for different annealing temperatures. Two main peaks were observed at the positions of the E^1_{2g} and A_{1g} modes, which represent the out-of-plane and in-plane vibration energies, which are indicators of the layers in the thin atomic films. The Raman spectra are very similar to that of MoS_2 from $(NH_4)_2MoS_4$ precursor[14,15]. Peaks were observed at 382.7 and 407.8 cm^{-1} for the E^1_{2g} and A_{1g} modes, respectively. As the growth temperature increased, the position of peak E^1_{2g} was blue-shift while the position of peak A_{1g} showed a red-shift. As a result, the frequency differences between the two peaks were 22, 24.3, and 25.1 cm^{-1} for annealing temperatures of 700, 900, and 1000 °C, respectively showing thicker layer with increasing growth temperature. This may be due to the different growth mechanisms of MoS_2 crystal at different temperatures[16].

Competition between the surface energy and interfacial energy results in structural changes from vertical growth and horizontal growth[16]. As solid precursors were decomposed below 800 °C, the MoS_2 layers grew layer by layer vertically and its structural dimension progressively transitioned to grow horizontally. At above 800 °C, the MoS_2 nano-crystals started to precipitate with the average grain size of crystals growing, thus forming honeycomb MoS_2. The peaks started to appear weakest at 500 °C and increased with the annealing temperature. The intensity of the peaks increased gradually, and the strongest intensity occurred at 1000 °C. After annealing at 1100 °C, the spin-coated MoS_2 precursor seemed to evaporate, and no peak was found in the Raman spectra. Therefore, controlling the annealing temperature is important to obtain crystalline MoS_2 layers during the annealing process.

Figure 2b shows the X-ray diffractometry (XRD) spectra of MoS_2 crystals with respect to the annealing temperatures. No peak was

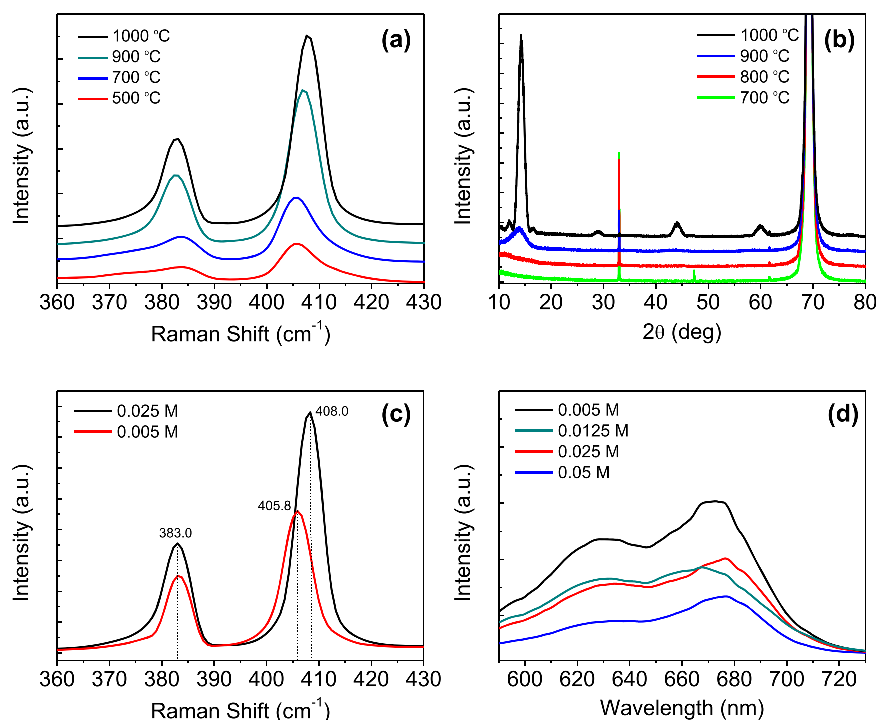

Fig. 2 Raman, XRD, and PL analyses. a Raman spectra and **b** XRD with annealing temperatures. **c** Raman spectra and **d** PL spectra with concentrations.

observed until 900 °C. A weak peak at $2\theta = 14.2°$ begins to appear at 900 °C, and there is a sharp increase at 1000 °C. Interestingly, more peaks appeared at $2\theta = 44.1°$, 59.5°, and 29.2° at 1000 °C. These peaks correspond to the (002), (004), (006), and (008) crystal planes of MoS_2, respectively[17]. The optimal annealing temperature for the DI water-based precursor solution is 1000 °C, and the greatest crystallinity appeared at this temperature. Several large peaks come from the silicon wafer, which were confirmed by the XRD results of MoS_2, SiO_2, and MoS_2 single crystals. All XRD peaks of MoS_2 crystallized at 1000 °C were well synthesized and matched well with the peak positions of a MoS_2 single crystal.

Supplementary Fig. 2a, b show the X-ray photoelectron spectroscopy (XPS) results of MoS_2 annealed at 1000 °C. The binding energy of the peaks at 232.2, 229.0, 226.2, 162.9, and 161.7 eV correspond to Mo $3d_{3/2}$, Mo $3d_{5/2}$, S 2S, S $2p_{1/2}$, and S $2p_{3/2}$, respectively. The binding energy corresponding to Mo-S crystal was assigned to $3d_{5/2}$ in Mo and $2p_{3/2}$ in the S peak[18]. There are two types of lattice structures of MoS_2: a 2H structure, in which the S atom is on the same line as Mo, and a 1T structure, in which the S atom is crossed around Mo. This structure changes the characteristics of the MoS_2. The 2H structure indicates semiconductor characteristics, but the 1T structure is quasi-metallic[1]. Due to the differences in the atomic structure, the binding energy is also different. The corresponding peaks confirmed that a 2H structure of MoS_2 was obtained from the DI water-based $(NH_4)_6Mo_7O_{24}{\cdot}4H_2O$ precursor[18,19].

The atomic ratio of Mo and S was confirmed by XPS results (Supplementary Table 1). Although the 1:2 ratio is ideal, the atomic ratio was actually 1:2.1–1:2.3 due to the characteristics of the synthesis. A higher precursor concentration results in a more ideal Mo-to-S ratio, and there might be more chance for each component to crystallize during the reaction. MoS_2 was synthesized without significant deviation of the atomic ratio, which confirms the reliability of the system for MoS_2 synthesis.

The Raman spectra were analyzed with precursor concentrations of 0.005 and 0.025 M, as shown in Fig. 2c. The peak positions in both E^1_{2g} and A_{1g} modes depend on the number of layers of MoS_2. Therefore, the number of layers can be counted using the frequency difference ($\Delta\kappa$) between E^1_{2g} and A_{1g} peaks. Comparing the peak positions with the spectrum obtained from other works[20–22], we predict that the spin-coated films are bi-layer ($\Delta\kappa = 22.8\ cm^{-1}$) and a few-layer ($\Delta\kappa = 25.0\ cm^{-1}$) structure for MoS_2 prepared from 0.005 and 0.025 M, respectively.

The photoluminescence (PL) spectra of MoS_2 thin films were obtained from various precursor concentrations using a 532-nm excitation laser, as shown in Fig. 2d. The peaks around 620 and 670 nm confirm the 2H structure of the synthesized MoS_2. Furthermore, as the number of layers decreases, the PL peak becomes stronger as the indirect band gap is converted to a direct band gap[19]. Therefore, as the concentration of the solution decreases, the number of layers of the synthesized MoS_2 decreases, resulting in strong PL peaks.

The morphology of several MoS_2 samples was observed using an optical microscope and atomic force microscopic (AFM) measurement after transferring the MoS_2 films to silicon wafers. Figure 3 shows MoS_2 layers that were spin-coated from three concentrations with the same spin conditions. It is clear that different concentrations can create visually distinct surfaces. The lowest concentration of 0.0065 M was unable to fully cover the substrate because the layer was too thin (Fig. 3a). Formulations with ≥0.0125 M resulted in full coverage because of the higher amount of solute. Nonetheless, 0.0125 M was the optimal concentration for spin coating, which can be seen in Fig. 3b. The resulting film has no holes, in contrast compared to the case of 0.0065 M and the free clusters that occurred with 0.025 M (Fig. 3c).

For smaller-scale observations, AFM images were captured from two $1 \times 1\text{-}\mu m^2$ MoS_2 samples made with 0.0125 and 0.025 M. A smoother surface was observed based on the root mean square roughness ($\mathbf{R_q}$) for the film prepared from 0.0125 M, which was about 0.18 nm, while for the film from higher concentration had $\mathbf{R_q}$ of around 0.20 nm (Fig. 3d, g). In Fig. 3e, h, the white dashed lines show the boundary between the MoS_2 and substrate in a $20 \times 20\ \mu m^2$ area. The yellow solid lines show the positions where

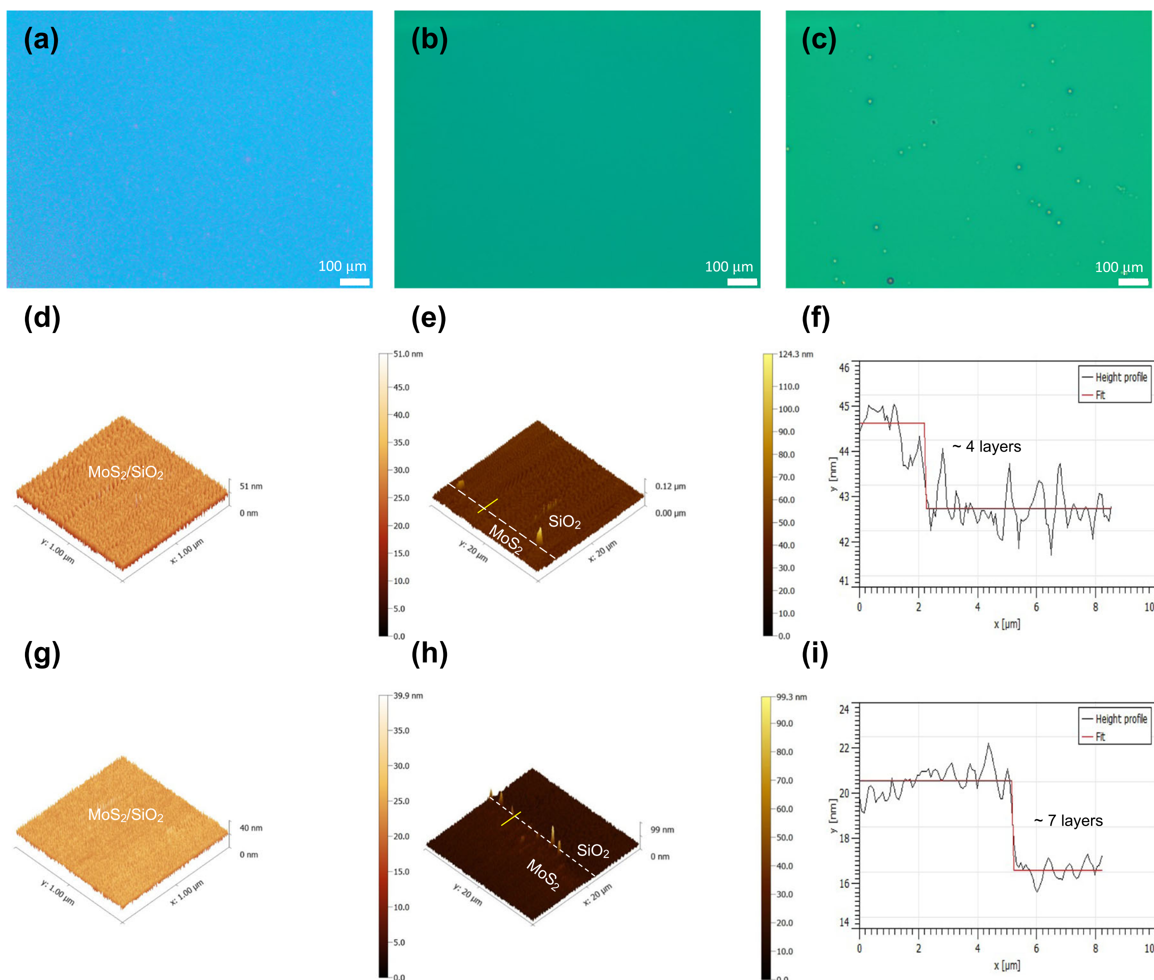

Fig. 3 AFM analyses of spin-coated MoS_2 films. a–c Optical images of spin-coated MoS_2 films from three concentrations: 0.0065, 0.0125, and 0.025 M, **d–f** AFM images and high profile of films from 0.0125 M and **g–i** 0.025 M (scale bar: 100 μm).

the MoS_2 thickness was evaluated. As shown in Fig. 3f, i, the height profiles measured along the chosen lines of the two MoS_2 films show that there were four and seven layers for 0.0125 and 0.025 M, respectively. These results were confirmed by Raman and high-resolution transmission electron microscopic (TEM) analyses. The thickness increased as the precursor concentration increased. The concentration of 0.0125 M was chosen to make an active layer for TFTs due to the thinner and smoother surface.

High annular dark-field (ADF) images were analyzed using scanning TEM (STEM) to obtain the detailed microstructures of MoS_2. We identified the number of layers from a cross-sectional TEM image. To do this, a carbon coating was placed on top of the MoS_2, and platinum was deposited to prepare it for focused ion beam analysis. Figure 4a shows the plan-view STEM image of large-scale MoS_2 layer. The plan view shows the grain boundaries between the multiple crystals that are formed during the annealing of the precursor solution. The inset of Fig. 4a is the selected area electron diffraction (SAED) pattern from inner to outer, corresponding to (100), (110), (200), (210), and (300) crystal planes. The sharp and bright diffraction rings of SAED implying the improvement of crystallinity after annealing at 1000 °C.

In Fig. 4b, the dark-field STEM image at high resolution confirms the arrangement of atoms in a penta-layered structure in the honeycomb field image. The image confirms that there is a 2H structure of MoS_2, which matches with the Raman spectra and XPS results[1]. Figure 4c shows low-resolution cross-sectional STEM image obtained with 0.0125 M. Figure 4d shows a high-resolution STEM image where the MoS_2 layer is divided into four layers. This was also confirmed by the AFM thickness measurement. Figure 4e shows high-resolution cross-sectional STEM images of MoS_2 obtained at 0.025 M. The white line is a part of a large connection of Mo atom where MoS_2 consists of about seven layers, which was confirmed by AFM.

Because the coating from DI water-based MoS_2 precursor had very good conditions, the synthesis was attempted on a larger substrate of $5 \times 5\,cm^2$ to verify the possibility of large-scale application. Figure 5a shows a picture of a transferred MoS_2 thin film on a new SiO_2 substrate after being synthesized with a large size of $5 \times 5\,cm^2$. The thin film of MoS_2 was large with good uniformity. This proves the possibility of using the bottom–up synthesis methods for large-size MoS_2 atomic layer formation with good uniformity.

To investigate the film transparency, MoS_2 films with different precursor concentrations were transferred on glass substrates, as shown in Fig. 5b. A lower concentration resulted in more transparency in the visible region because of the smaller number of layers, as shown in Fig. 5c. The transmission at 550 nm was 46.2, 59.7, 80.1, and 85.5% for concentrations of 0.005, 0.025, 0.0125, and 0.005 M, respectively. The transparency peaks are related to the band structure of MoS_2 films, and there are some red-shifts in the range above 600 nm, which are related to the increase of PL spectra[7,18,23]. Compared to the previous $(NH_4)_2MoS_4$ precursor, this DI water-based $(NH_4)_6Mo_7O_{24}{\cdot}4H_2O$ precursor solution could

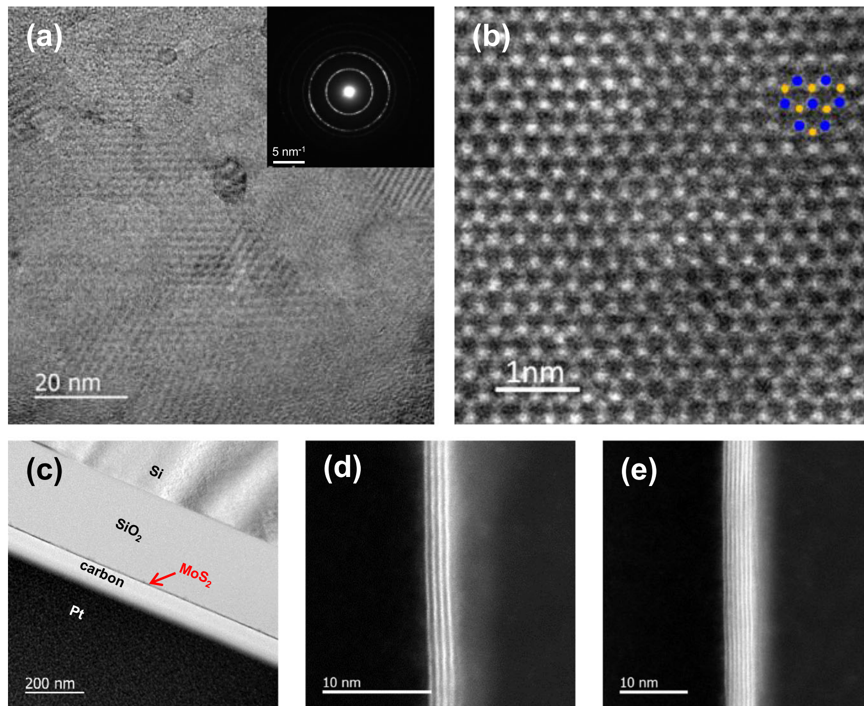

Fig. 4 TEM analyses of MoS_2 atomic films. **a** ADF-STEM plan view with corresponding SAED pattern; **b** high-resolution dark-field STEM plan view of 0.0125 M MoS_2; Mo and S atoms are marked as blue and orange colors, respectively. **c** Low-resolution and **d** high-resolution STEM cross-sectional view of 0.0125 M of MoS_2 and **e** high-resolution STEM cross-sectional view of 0.025 M of MoS_2.

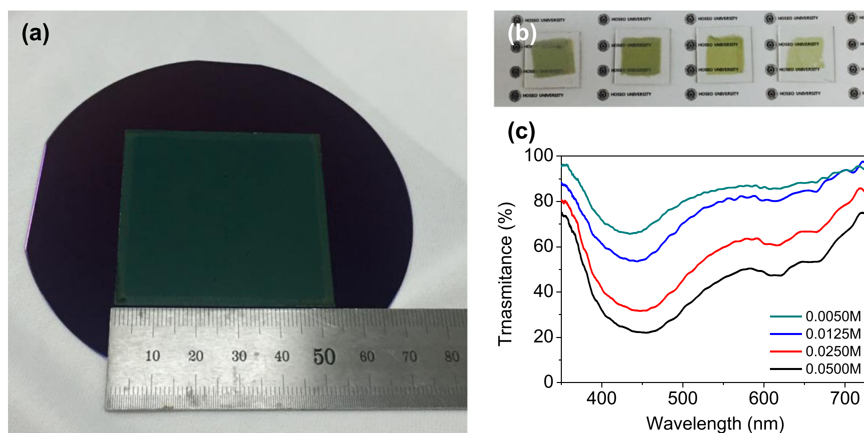

Fig. 5 Transferred MoS_2 and transmittance property. **a** Transferred MoS_2 of 5 × 5 cm on a substrate, **b** transferred MoS_2 with various concentrations on glass substrate, and **c** transmittance of MoS_2 thin films on glass with concentrations.

make rather simple and consistent coatings, but the coating is a little thicker and provides more atomic layers in films.

Electrical characteristics of MoS_2 thin-film transistors

TFTs were fabricated with the DI water-based synthesized MoS_2 as a semiconducting layer to evaluate the electrical properties. To form the S/D electrodes on the MoS_2 layer, Al was used instead of Ti/Au unlike in previous publications[10,12], because the Fermi level of Al, as a cheap material, is close to the conduction band of MoS_2[6]. EHD jet-printed Ag was applied to MoS_2 TFTs on two gate dielectrics because of the similar energy level of Ag and Ti. The detailed EHD jet printing of Ag paste jetting is described in Supplementary Note 1.

The TFTs were prepared depending on the insulator layer and deposition methods with the same channel length and width of 140 and 1500 μm, respectively, as shown in Fig. 6a. This resulted in 4 groups of 15 devices each. In our experiments, our water-soluble MoS_2 precursor using a spin-coating method with high successful patterning electrodes (100% for thermal evaporated Al, 90% for EHD jet printed Ag) did show that the device manufacture yield was very good. We can thus predict that the homogenous and large-scale MoS_2 based on our water-soluble MoS_2 would facilitate a high manufacture yield of devices.

Figure 6 shows the transfer and output characteristic curves of spin-coated MoS_2 TFTs. Figure 6b, c show the transfer properties for device groups A and B with SiO_2 dielectric. V_{GS} was varied from −20 to 100 V and V_{DS} was kept at 10 V for the SiO_2 gate insulator, while V_{GS} of −5 to 40 V and V_{DS} of 1 V were applied for the Al_2O_3

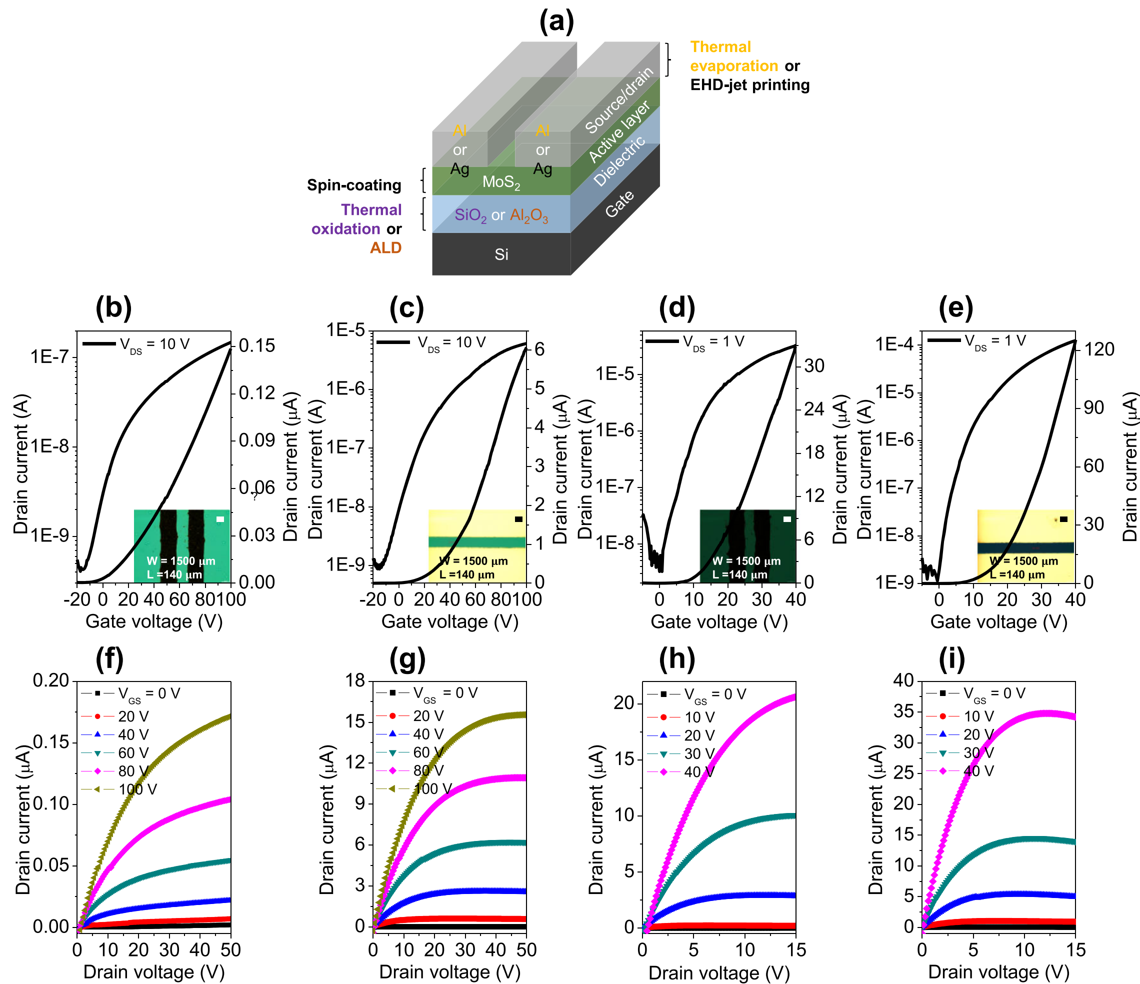

Fig. 6 Schematic and electrical properties of MoS_2 TFTs. **a** Schematic and the composition of MoS_2 TFTs with layer roles and deposition methods of four groups. **b**–**e** Typical transfer characteristics and **f**–**i** output curves of TFTs from groups A, B, C, and D, respectively. The inset of **b**–**e** shows optical image of a representative TFT for each group (scale bar: 100 μm).

Table 1. Electrical properties of solution-processed MoS_2 TFTs with device configurations.

Device group	[a]Device structures	I_{on}/I_{off}	V_{th} [V]	S–S [V dec^{-1}]	μ_{lin} [cm^2 V^{-1} s^{-1}]
A	Printed Ag/MoS_2/SiO_2/Si wafer	$(2.5 \pm 2.5) \times 10^2$	20 ± 3	17.3 ± 2.5	0.008 ± 0.003
B	Evaporated Al/MoS_2/SiO_2/Si wafer	$(0.9 \pm 1.6) \times 10^3$	32 ± 5	10.5 ± 1.8	0.09 ± 0.03
C	Printed Ag/MoS_2/Al_2O_3/Si wafer	$(1.3 \pm 4.5) \times 10^4$	17 ± 2.5	6.6 ± 0.8	2.1 ± 0.5
D	Evaporated Al/MoS_2/Al_2O_3/Si wafer	$(0.8 \pm 0.3) \times 10^5$	21 ± 1.4	2.3 ± 0.2	7.9 ± 0.6

[a]Device configurations: A: EHD jet-printed Ag (2000 nm)/MoS_2 (2.6 nm)/SiO_2 (300 nm)/Si wafer, B: thermal-evaporated Al (100 nm)/MoS_2 (2.6 nm)/SiO_2 (300 nm)/Si wafer, C: EHD jet-printed Ag (2000 nm)/MoS_2 (2.6 nm)/Al_2O_3 (80 nm)/Si wafer, D: thermal-evaporated Al (100 nm)/MoS_2 (2.6 nm)/Al_2O_3 (80 nm)/Si wafer.

insulator (Fig. 6d, e) due to the different dielectric materials with different breakdown voltages.

The inset of each transfer curve figure shows a representative top–view microscope image for each typical device group. All devices express pronounced n-type MoS_2 behavior. The field-effect mobility (μ_{eff}) of TFTs was extracted from the linear region using the conventional equation at a fixed V_{DS} (1 V for Al_2O_3 and 10 V for SiO_2 cases). The peak mobility values of MoS_2 devices are 0.011, 0.12, 2.6, and 8.5 cm^2 V^{-1} s^{-1} for groups A–D, respectively, as summarized in Table 1.

It is very interesting that remarkable improvement was observed in the performance of TFTs as the gate dielectric changed from SiO_2 to Al_2O_3, and there was reasonable improvement when changing S/D electrodes from printed Ag to evaporated Al. The mobility differences are over 70 times after switching gate dielectric from low-k SiO_2 to high-k dielectric Al_2O_3. The on-to-off current ratio ranges also improved as 10^4–10^5 for Al_2O_3 dielectric and $<10^4$ for SiO_2.

All MoS_2 TFTs exhibit both linear and saturation regions (Fig. 6f–i). The output curves at several gate voltages after sweeping the drain voltage confirm the typical behavior of MoS_2. It is clear that a better Ohmic contact property obtained in low V_{DS} output curves in the case of Al S/D electrodes. As shown in Fig. 6f, h, the drain–source current of devices is linear at low drain–source

voltages and saturates as V_{DS} increases in the low gate-voltage range. There is less saturation at higher gate voltages for the case of printed Ag. For the cases of Al S/D electrodes in Fig. 6g, i, even at low or high gate voltage, output curves of devices show good contact and are linear at low V_{DS}, but there is more solid saturation at high V_{DS}.

Two reasons could explain the results derived from the TFT characterization. First, the carrier mobility of MoS_2 TFTs with printed Ag electrodes is quite low compared to TFTs with thermal-evaporated Al. This is probably due to poor charge injection from Ag electrodes to the MoS_2 layer, even though equivalent low Schottky barrier heights for electrons could be derived from both metals. There is poor charge diffusion from the top layer of Ag to the underlying layer and channel because of the less dense texture and porous structure of Ag layer, as observed in SEM and AFM (Supplementary Fig. 3). Less contact and conduction problems between printed S/D and MoS_2 are expected because of any residues that formed at the relatively low sintering temperature of 150 °C. Although the TFTs with the EHD jet-printed Ag S/D shows limited performance, the printing technique makes devices based on MoS_2 or even other 2D materials possible with a low-cost process.

Second, the MoS_2 TFT with high-*k* Al_2O_3 ($k = 7$) exhibits outstanding electrical characteristics compared with TFTs based on low-*k* SiO_2 ($k = 3.9$). These improved properties can be explained by the screening effect from the high-*k* dielectric, which can damp Coulomb scattering from charged impurities. In addition, enhanced performance of the MoS_2 TFT is also attributed to the smooth surface at the MoS_2/Al_2O_3 interface after transferring, as observed in AFM. Much improved properties can be achieved for solution-processed MoS_2 from dielectric engineering.

It is worth noting that our water-based MoS_2 transistors without a post-annealing step or encapsulation exhibited linear mobility up to 8.5 $cm^2 V^{-1} s^{-1}$ that is really improved compared to our similar approach but different solution base[10] and much higher than that of some other solution process[24,25]. This is comparable with those of previous publications proposed by other solution approach on sapphire[9,26] and seeded growth method[27], which needed complex process and chemical treatments with additional sulfur. This result was even higher than that of CVD-grown monolayer MoS_2 with ink-jet printed Ag as the S/D[12], multi-step CVD-grown MoS_2 with expensive Au electrodes[28] and some based on CVD[29,30]. Supplementary Table 2 shows details about mobility and current ratio of our devices compared with those previously reported in the literature. Our MoS_2 TFT system may face many obstacles for high performance because of the solution process, such as water or oxygen absorption, intrinsic structural defects (point defects and grain boundaries), and interfacial issues among semiconductor and gate dielectric and S/D. Nevertheless, we believe that our method will facilitate major developments for 2D MoS_2 materials in low-cost printed electronic applications.

DISCUSSION

In this study, a new DI water-based formulation for MoS_2 was successfully developed using a precursor of $(NH_4)_6Mo_7O_{24}{\cdot}4H_2O$ as Mo source and sulfur solution as S source. The DI water-based precursor solution was spin-coated and be converted to MoS_2 thin film by one-step annealing without CVD sulfurization. The synthesized MoS_2 layer could be fabricated with large size over 4″, good uniformity, and transparency in a 2H MoS_2 structure, which was confirmed by analytical methods. The synthesized MoS_2 had a smooth and homogeneous surface when being spin-coated from a solution concentration of ≥0.0125 M. The resulting MoS_2 layers were 4 and 7 with 0.0125 and 0.025 M precursor solution, respectively. Therefore, the atomic layers of MoS_2 can be controlled by the concentration of the DI water-based precursor.

Four TFT groups were prepared with MoS_2 semiconductor, Al, and EHD jet-printed Ag S/D electrodes on different dielectrics. The solution-processed MoS_2 TFT on Al_2O_3 gate dielectric with Al S/D electrodes shows improved electrical properties, such as a mobility of 8.5 $cm^2 V^{-1} s^{-1}$ and an on–off ratio of about 1.0×10^5. Solid saturation with good contact can also be obtained from all MoS_2 TFTs in output characteristics. The simple and environment friendly water-based solution method could open the new pathway for low-cost preparation of other TMDC thin films in next-generation electronics.

METHODS

Materials and solution preparation

In this work, precursor solution for spin-coating MoS_2 with several concentrations (0.005–0.05 M) were prepared from Mo and S precursor solution source. Mo solution and S solution were dissolved separately using different relevant solvents, which were 5 mL DI water (for Mo) and 10 mL ethanolamine accompanied with carbon disulfide (for S). CS_2 with a small amount of 1 mL played an important role to help dissolve well S powder in ethanolamine and to make S-rich solution as well. Then two source solutions were mixed together with the ratio of 1 Mo:2 S (wt%) to get final precursor solution.

To obtain uniform thin films, the solution should sufficiently wet the SiO_2/Si substrate. Thus, the substrate was treated with UV/O_3 for 30 min to improve the wettability. The MoS_2 precursor solution was spin-coated at 3000 rpm for 30 s and then pre-baked at 150 °C for 30 min. Subsequently, the films were heated in a quartz tube furnace at elevated temperatures ranging from 500 to 1000 °C at a ramp rate of 15 °C min^{-1} for 1 h to obtain MoS_2 films. The growth of MoS_2 inside furnace was under low vacuum (~10^{-2} Torr) after removing air.

Fabrication of MoS_2 thin-film transistors

To investigate the translation of the synthesized MoS_2 to electronic applications, MoS_2 TFTs with bottom-gate and top-contact structure were fabricated on 300-nm-thick SiO_2 or 80-nm Al_2O_3 as the gate insulator. The $(NH_4)_6Mo_7O_{24}{\cdot}4H_2O$ precursor layer was created by a spin-coating technique with a 0.0125 M precursor solution after UV/O_3 treatment to improve wetting. The precursor was annealed at 1000 °C of tubular furnace to obtain a crystalline MoS_2 thin-film layer. The S/D electrodes of the TFT were fabricated by depositing 100-nm-thick Al using thermal evaporation with shadow masks or EHD jet-printed Ag for comparison.

Silver paste was modified by mixing 100 parts of the original Ag paste (4000 pcs, AD-V7-108) with 1 part of Silveray solvent and 3 parts of propylene glycol methyl ether acetate (PGMEA, Sigma Aldrich) based on our recent publication[13]. As an alternative dielectric, 80 nm of Al_2O_3 was deposited on a silicon wafer using atomic layer deposition. As-grown MoS_2 layers were transferred onto Al_2O_3/Si substrate to fabricate TFTs using a conventional wetting method with the support of polymethyl methacrylate (PMMA)[10].

Next, silver paste was printed in Taylor cone jet mode on both as-grown and transferred MoS_2 films using an EHD jet printer, followed by drying for 30 min at 150 °C on a hot plate to form the S/D electrodes of the TFTs. More detail about EHD jet printing is addressed in Supplementary Note. The procedure of the TFT fabrication and a cross-sectional view of devices are shown in Figs. 1 and 6a.

Characterization of MoS_2 thin films and devices

The synthesized MoS_2 thin films were analyzed by Raman spectroscopy, XRD, UV-Vis spectroscopy, AFM (Nano expert II EM4SYS), and XPS. Atomic-resolution ADF-STEM (JOEL-ARM 200F) was used to obtain atomic images and observe the microstructure with a spherical aberration corrector (CEOS GmbH) at 200 K. The semi-angles of the ADF detector were changed from 90 to 200 mrad with a scan rate of 6 μm $pixel^{-1}$ and 512×512 pixels per frame.

TEM samples were prepared using a transfer technique on the synthesized MoS_2 with PMMA on a Cu mesh coated with a grid of lacey carbon. For the preparation of transparent samples, MoS_2 was transferred to a glass substrate using a conventional PMMA method. A parameter analyzer (Keithley 4200) was used to characterize the electrical properties of the MoS_2 TFT in a dark room at room temperature.

DATA AVAILABILITY

The data are available from corresponding author upon reasonable request.

Received: 21 November 2020; Accepted: 9 September 2021;
Published online: 11 October 2021

REFERENCES

1. Chhowalla, M. et al. The chemistry of two-dimensional layered transition metal dichalcogenide nanosheets. *Nat. Chem.* **5**, 263–267 (2013).
2. Jariwala, D., Sangwan, V. K., Lauhon, L. J., Marks, T. J. & Hersam, M. C. Emerging device applications for semiconducting two-dimensional transition metal dichalcogenides. *ACS Nano* **8**, 1102–1120 (2014).
3. Wang, S. et al. Shape evolution of monolayer MoS_2 crystals grown by chemical vapor deposition. *Chem. Mater.* **26**, 6371–6379 (2014).
4. Tarasov, A. et al. Highly uniform trilayer molybdenum disulfide for wafer-scale device fabrication. *Adv. Funct. Mater.* **24**, 6389–6400 (2014).
5. Choi, W. et al. Recent development of two-dimensional transition metal dichalcogenides and their applications. *Mater. Today* **20**, 116–130 (2017).
6. Liu, K. K. et al. Growth of large-area and highly crystalline MoS_2 thin layers on insulating substrates. *Nano Lett.* **2**, 1538–1545 (2012).
7. Yang, J. et al. Wafer-scale synthesis of thickness-controllable MoS_2 films via solution-processing using a dimethylformamide/n-butylamine/2-aminoethanol solvent system. *Nanoscale* **7**, 9311–9319 (2015).
8. Park, S. et al. Layer-selective synthesis of MoS_2 and WS_2 structures under ambient conditions for customized electronics. *ACS Nano* **14**, 8485–8494 (2020).
9. Gomes, F. O. V. et al. High mobility solution processed MoS_2 thin film transistors. *Solid State Electron.* **158**, 75–84 (2019).
10. Kwack, Y. J. & Choi, W.-S. CVD-free S-rich solution-process for two-dimensional MoS_2 atomic layer films. *Nanotechnology* **30**, 385201 (2019).
11. Can, T. T. Thuy, Kwack, Y. J. & Choi, W.-S. Drop-on-demand patterning of MoS_2 using electrohydrodynamic jet printing for thin-film transistors. *Mater. Des.* **199**, 109408 (2020).
12. Kim, T. Y. et al. Electrical properties of synthesized large-area MoS_2 field-effect transistors fabricated with inkjet-printed contacts. *ACS Nano* **10**, 2819–2826 (2016).
13. Can, T. T. T., Nguyen, T. C. & Choi, W.-S. Patterning of high-viscosity silver paste by an electrohydrodynamic-jet printer for use in TFT applications. *Sci. Rep.* **9**, 9180 (2019).
14. Kim, J., Higashimine, K., Haga, K. & Tokumitsu, E. Fabrication of MoS_2 thin films on oxide-dielectric-covered substrates by chemical solution process. *Phys. Status Solidi* **254**, 1600536 (2017).
15. Brito, J. L., Ilija, M. & Hernández, P. Thermal and reductive decomposition of ammonium thiomolybdates. *Thermochim. Acta* **256**, 325–338 (1995).
16. Fei, L. et al. Direct TEM observations of growth mechanisms of two-dimensional MoS_2 flakes. *Nat. Commun.* **7**, 12206 (2016).
17. Shasha, L. et al. Preparation of MoS_2 nanofibers by electrospinning. *Mater. Lett.* **73**, 223–225 (2012).
18. Brown, N. M. D., Cui, N. & Mckinley, A. An XPS study of the surface modification of natural MoS_2 following treatment in an RF-oxygen plasma. *Appl. Surf. Sci.* **134**, 11–21 (1998).
19. Lee, Y., Lee, J., Bark, H. & Oh, I.-K. Synthesis of wafer-scale uniform molybdenum disulfide films with control over the layer number using a gas phase sulfur precursor. *Nanoscale* **6**, 2821 (2014).
20. Kwon, H. et al. Monolayer MoS_2 field-effect transistors patterned by photolithography for active matrix pixels in organic light-emitting diodes. *npj 2D Mater. Appl.* **3**, 9 (2019).
21. Yu, Y. et al. Controlled scalable synthesis of uniform, high-quality monolayer and few-layer MoS_2 films. *Sci. Rep.* **3**, 1–6 (2013).
22. Zhan, Y., Liu, Z., Najmaei, S., Ajayan, P. M. & Lou, J. Large-area vapor-phase growth and characterization of MoS_2 atomic layers on a SiO_2 substrate. *Small* **8**, 966–971 (2012).
23. Vikraman, D., Akbar, K., Hussain, S. & Yoo, G. Direct synthesis of thickness-tunable MoS_2 quantum dot thin layers: optical, structural and electrical properties and their application to hydrogen evolution. *Nano Energy* **35**, 101–114 (2017).
24. Li, J., Naiini, M. M., Vaziri, S., Lemme, M. C. & Östling, M. Inkjet printing of MoS_2. *Adv. Funct. Mater.* **24**, 6524–6531 (2014).
25. George, A. S. et al. Wafer scale synthesis and high resolution structural characterization of atomically thin MoS_2 layers. *Adv. Funct. Mater.* **24**, 7461–7466 (2014).
26. Lin, Z. et al. Solution-processable 2D semiconductors for high-performance large-area electronics. *Nature* **562**, 254–258 (2018).
27. Han, G. H. et al. Seeded growth of highly crystalline molybdenum disulphide monolayers at controlled locations. *Nat. Commun.* **6**, 6128 (2015).
28. Heo, S., Hayakawa, R. & Wakayama, Y. Carrier transport properties of MoS_2 field-effect transistors produced by multi-step chemical vapor deposition method. *J. Appl. Phys.* **121**, 024301 (2017).
29. Park, I. J. et al. Stretchable thin-film transistors with molybdenum disulfide channels and graphene electrodes. *Nanoscale* **10**, 16069 (2018).
30. Conti, S. et al. Low-voltage 2D materials-based printed field-effect transistors for integrated digital and analog electronics on paper. *Nat. Commun.* **11**, 3566 (2020).

ACKNOWLEDGEMENTS

This work was supported by the Basic Science Research Program through the National Research Foundation Korea (NRF-2018R1D1A1B07048441).

AUTHOR CONTRIBUTIONS

Y.-J.K. designed precursor solution and characterization. T.T.T.C. designed, fabricated, and characterized the devices and wrote the manuscript. W.-S.C. guided the project and wrote the manuscript. All authors reviewed the manuscript.

COMPETING INTERESTS

The authors declare no competing interests.

ADDITIONAL INFORMATION

Supplementary information The online version contains supplementary material available at https://doi.org/10.1038/s41699-021-00264-7.

Correspondence and requests for materials should be addressed to Woon-Seop Choi.

Reprints and permission information is available at http://www.nature.com/reprints

Publisher's note Springer Nature remains neutral with regard to jurisdictional claims in published maps and institutional affiliations.

Open Access This article is licensed under a Creative Commons Attribution 4.0 International License, which permits use, sharing, adaptation, distribution and reproduction in any medium or format, as long as you give appropriate credit to the original author(s) and the source, provide a link to the Creative Commons license, and indicate if changes were made. The images or other third party material in this article are included in the article's Creative Commons license, unless indicated otherwise in a credit line to the material. If material is not included in the article's Creative Commons license and your intended use is not permitted by statutory regulation or exceeds the permitted use, you will need to obtain permission directly from the copyright holder. To view a copy of this license, visit http://creativecommons.org/licenses/by/4.0/.

© The Author(s) 2021